Calculations of the ferromagnet-to-spin-glass transition in diluted magnetic systems with an RKKY interaction

P.J.T. Eggenkamp and H.J.M. Swagten
Department of Physics, Eindhoven University of Technology, P.O. Box 513, NL-5600 MB Eindhoven, The Netherlands

T. Story
Institute of Physics, Polish Academy of Sciences, aleja Lotników 32/46, PL-02-668 Warsaw, Poland

V.I. Litvinov
Institute of Material Science Problems, Ukrainian Academy of Sciences, 5 Wilde Street, 274001 Chernovtsy, Ukraine

C.H.W. Swüste and W.J.M. de Jonge
Department of Physics, Eindhoven University of Technology, P.O. Box 513, NL-5600 MB Eindhoven, The Netherlands
(Received 12 January 1995)

The transition temperatures and phase diagram of a diluted magnetic system with a Ruderman-Kittel-Kasuya-Yosida (RKKY) interaction are studied by extension of the model by Sherrington and Southern. The model provides a way to calculate the distribution of interactions in the material. Some of these distributions are presented. Using the mean and the width of the distributions, the magnetic transition temperatures can be calculated. Furthermore, the phase boundary separating the ferromagnetic state from the spin-glass state can be determined. The results are compared with experimental data obtained for $Sn_{1-x}Mn_xTe$ and $Pb_{0.28-x}Sn_{0.72}Mn_xTe$. In these compounds the magnetic phase depends on both the manganese concentration and the concentration of free carriers. Therefore, these compounds are very suitable to study the RKKY interaction. The calculated transition temperatures can describe the experimental results only qualitatively, whereas the calculated phase boundaries are quantitatively in accordance with the experimental data.

I. INTRODUCTION

In diluted magnetic systems the magnetic phase is usually determined by the concentration of magnetic ions. At low concentrations of magnetic ions most systems are spin glasses, whereas at higher concentrations a ferromagnetic or antiferromagnetic phase occurs. This behavior can be explained with the interaction mechanisms present in the material. In insulators, like $Eu_xSr_{1-x}S$,[1] and semiconductors, like $Zn_{1-x}Mn_xSe$ or $Cd_{1-x}Mn_xTe$,[2–5] the important interactions are direct exchange[6] and superexchange.[7] If a competition between these interactions occurs due to the lattice topology or a different sign of the interactions, a spin-glass phase is expected at low concentrations of magnetic ions. At high concentrations of the magnetic ions, the magnetic phase of the compound is determined by the strongest of the interactions, which usually is the interaction with the nearest neighbor.

In metallic systems, like *Cu*Mn or *Au*Fe,[8,9] the most important interaction is the long-ranged Ruderman-Kittel-Kasuya-Yosida (RKKY) interaction.[10] This interaction is oscillating as a function of the distance between two magnetic ions, thereby inducing both ferromagnetic and antiferromagnetic interactions in the material, which leads to a spin-glass phase. At high concentrations of magnetic ions, a ferromagnetic or antiferromagnetic phase occurs, depending on the strongest interaction. The strongest interaction may be determined by the RKKY interaction, but additional interaction mechanisms, like superexchange or direct exchange, may also play a role.[11] If at these high concentrations the material is ferromagnetic, like in *Au*Fe, an intermediate phase, called the reentrant-spin-glass phase, may be observed.[12] In a reentrant-spin-glass phase two phase transitions are observed: a ferromagnetic transition at a higher temperature and a spin-glass transition at a lower temperature.

In the semimetallic system of $Sn_{1-x}Mn_xTe$ and $Pb_{0.28-x}Sn_{0.72}Mn_xTe$ the situation is even more diverse. Like in *Au*Fe, ferromagnetic, spin-glass, and reentrant-spin-glass phases are observed, but the material does not always show a phase transition within the experimental temperature range ($T > 1.5$ K, paramagnetic phase). Most importantly, the occurrence of these magnetic phases not only depends on the manganese concentration, but also on the concentration of free carriers in the material. This carrier concentration can be controlled by a thermal annealing procedure, independent of the manganese concentration.[13,14] In terms of interaction mechanisms, the system represents an intermediate situation between semiconductors and metals, because both the superexchange and the RKKY interaction are important. This can qualitatively explain the observed magnetic behavior (see Sec. II).

The first quantitative theoretical approach to the carrier-induced ferromagnetic-to-spin-glass transition was based on some geometrical arguments to predict the

phase transition.[13] An improvement of this argument will be presented in this paper (see Sec. VI). Subsequently, the phase boundary was described with the model of Sherrington and Kirkpatrick (SK),[15] which is often used to describe spin glasses, but can also describe a transition to a ferromagnetic state. In the SK model, the magnetic system is described by the Heisenberg Hamiltonian

$$\mathcal{H} = -\sum_{i,j} J_{ij} \boldsymbol{S}_i \cdot \boldsymbol{S}_j, \tag{1}$$

in which each ion is assumed to interact with all other ions. The interaction strength J_{ij} is assumed to have a Gaussian probability distribution. Whenever the width (ΔJ) of the distribution is larger than its mean (J_0), the model predicts a spin-glass phase. Instead of these Gaussian distributions, the distributions of internal fields were calculated using the mean random field (MRF) model.[16] The mean and width of these distributions were used to calculate the phase boundary.[17,18] Since the MRF model neglects the discreteness of the lattice, a discrete version of this model was also formulated, but this lacked a firm basis.[18] This basis can be provided by the model by Sherrington and Southern (SS).[19] This model is the quantum, general spin version of the well-known short-range model by Edwards and Anderson.[20] In the present contribution, we will use the extension of the model, appropriate for systems with a large number of magnetic neighbors, as suggested by SS. In our opinion, the SS model describes the situation encountered in diluted systems in a more realistic way than the SK model, because the range of the interaction is strongly limited by the carrier mean free path, whereas SK assume an infinite range of the interaction.

Moreover, we will apply the model for the theoretical calculation of the transition temperatures. In spin-glass systems such calculations have been reported by several authors. Both SS and SK have given relations for the transition temperatures. However, the spin-glass ordering temperature observed in computer simulations is much lower than the ordering temperature predicted by SK.[21] Mydosh and Nieuwenhuys[8,22] have described the T-x phase diagram of AuFe and PdMn with calculations based on the MRF and SK models. These calculations could describe the qualitative features of the experimental data. Nevertheless, these authors conclude that the SK model cannot be used in their case for a quantitative description. Larsen[23] has developed a model to describe the spin-glass freezing temperatures, rendering fair agreement with the experimental data on CuMn and AuFe. However, he assumes that the width of the distribution of interactions is given by the envelope of the RKKY function, and thereby depends on the distance between impurities. The validity of this assumption is questionable.

In this paper we will describe the magnetic properties of diluted magnetic systems with a RKKY interaction. Using the SS model, we will calculate the distribution of interactions in the material (Sec. III), the transition temperatures (Sec. V), and the dependence of the phase transition on the concentration of magnetic ions and free carriers (Sec. VI). The influence of nonmagnetic disorder, causing a reduction of the mean free path of carriers, will be introduced in the model (Sec. III) and discussed. Before the results of the calculations will be presented, a brief review of the experimental results will be given (Sec. II). The paper will be completed with a summary of the results and the conclusions (Sec. VII).

II. EXPERIMENTAL RESULTS AND PHASE DIAGRAM

In order to compare our model to experimental results, we will first shortly describe the magnetic-phase diagram of $Sn_{1-x}Mn_xTe$ and $Pb_{0.28-x}Sn_{0.72}Mn_xTe$. The low-temperature magnetic phase of these compounds was studied on bulk samples with a manganese concentration ranging from $x = 0.007$ to $x = 0.10$, and a carrier concentration p covering the broad range between 10^{20} and 4×10^{21} cm^{-3}. The carrier concentration was determined from measurements of the Hall effect at 77 K. Since it was shown that the carrier concentration in $Pb_{0.28-x}Sn_{0.72}Mn_xTe$ is constant below 100 K,[24] we can assume that the value found at 77 K is also valid at liquid-helium temperatures. In the spirit of Karczewski *et al.*,[25] we have corrected the Hall-carrier densities for the band structure of the compound to yield the true carrier concentration. This correction factor was between 0.8 and 1.5.

The experiments to determine the magnetic phase of the samples included magnetization, ac susceptibility, specific heat,[13,17,24,26–28] and neutron diffraction.[14] The resulting magnetic-phase diagram is presented in Fig. 1. In this diagram, the magnetic phase of a sample is in-

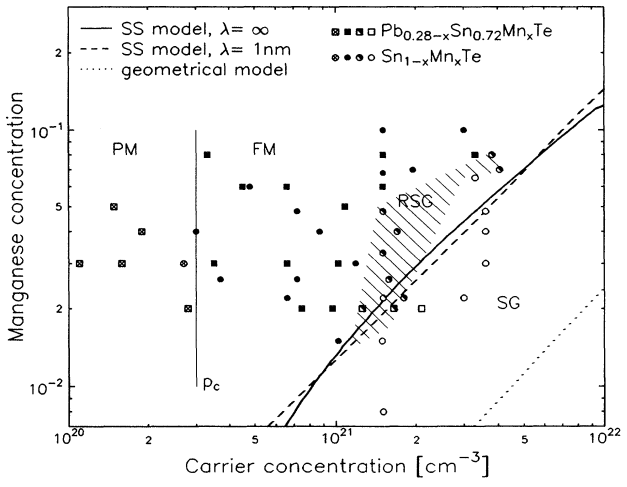

FIG. 1. Magnetic-phase diagram of $Pb_{0.28-x}Sn_{0.72}Mn_xTe$ and $Sn_{1-x}Mn_xTe$. The squares represent measurements on $Pb_{0.28-x}Sn_{0.72}Mn_xTe$; the circles represent measurements on $Sn_{1-x}Mn_xTe$. Crossed symbols, paramagnets; solid symbols, ferromagnets; half-solid symbols, reentrant spin glasses; and open symbols, spin glasses. The curves represent the calculations of the phase boundary. Solid curve, SS model, mean free path $\lambda = \infty$; dashed curve, SS model, $\lambda = 1$ nm; dotted curve, geometrical model.

dicated as a function of both the manganese concentration and the carrier concentration. It is evident that the carrier concentration has a profound effect on the magnetic phase of the material. At a carrier concentration of $p_c = 3 \times 10^{20}$ cm^{-3} an abrupt change in the magnetic phase, measured at $T > 1.5$ K, from a paramagnetic to a ferromagnetic state takes place. This transition, which was first found by Story *et al.*,[29] is imposed by the band structure of the material.[30]

If the concentration of carriers is increased further, however, the oscillations in the RKKY interaction become important. At high carrier concentrations ($p \gg p_c$), this period is shorter and antiferromagnetic interactions start to compete with the ferromagnetic interactions, inducing a spin-glass state. This transition to the spin-glass state is a gradual transition, and an intermediate phase, the reentrant-spin-glass phase, is also observed.[14] A sample is considered a reentrant spin glass if in the experimental temperature range ($T > 1.5$ K) two transitions were observed. The reentrant-spin-glass regime is indicated by the hatched region in Fig. 1. The location of this carrier-concentration-induced transition in the phase diagram also depends on the manganese concentration, as it is shifted to higher carrier concentrations if the manganese concentration is increased. In this paper, we will try to explain the ferromagnetic-to-spin-glass transition, as well as the transition temperatures based on the SS model, which will be introduced in the next section.

III. SS MODEL AND RKKY INTERACTION IN $Pb_{1-x-y}Sn_yMn_xTe$

In the Heisenberg Hamiltonian [Eq. (1)], Sherrington and Southern have assumed that the interaction strength is distributed according to a Gaussian distribution, with mean J_0 and width ΔJ, for a limited number of neighbors. They calculated the temperatures at which the transition from the paramagnetic to the ferromagnetic state (Curie temperature T_C) and from the paramagnetic to the spin-glass state (T_{SG}) occur:

$$T_C = \frac{S(S+1)J_0}{3k_B}\left\{1+\left[1-\frac{3}{S(S+1)}\left(\frac{\Delta J}{J_0}\right)^2\right]^{1/2}\right\} \tag{2a}$$

and

$$T_{SG} = \frac{2\Delta J}{3k_B}\left\{S^2(S+1)^2 + S(S+1)/2\right\}^{1/2}. \tag{2b}$$

In Fig. 2 the transition temperatures, reduced to the width of the distribution and taking $S = 5/2$, are shown as a function of the parameter $\eta = J_0/\Delta J$. The material is expected to show the transition with the highest transition temperature. A change of the magnetic phase is therefore expected when $T_{SG} = T_C$, yielding $\eta = 40/\sqrt{1295} \approx 1.1$.

For a real system, SS have suggested that one should take

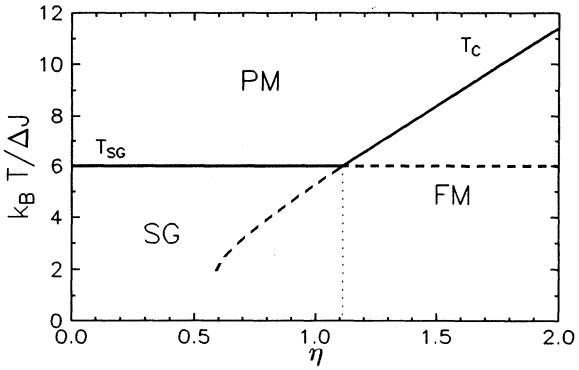

FIG. 2. Sherrington-Southern (Ref. 19) phase diagram. The diagram shows the transition temperatures versus the ratio of the mean and the width of the distribution. T_{SG}, transition temperature from the paramagnetic (PM) to the spin-glass (SG) state; T_C, transition temperature from the PM to the ferromagnetic (FM) state.

$$J_0 = \sum_i J(R_{ij}) \tag{3a}$$

and

$$(\Delta J)^2 = \sum_i \left[J(R_{ij}) - J_0\right]^2, \tag{3b}$$

where the summation runs over all manganese ions present in the material. These equations will be used to calculate the transition temperatures and subsequently the phase boundary.

In these equations, the RKKY interaction will be inserted. As mentioned in Sec. II, the RKKY interaction is only effective for carriers in the Σ band. This band is, however, 12-fold degenerate. Therefore, the total carrier concentration must be divided over these 12 subbands. Considering the Σ band to be parabolic, the RKKY interaction becomes

$$J_{RKKY}(R) = \frac{m^* J_{sd}^2 a_0^6 k_F^4 N_\Sigma}{32\pi^3\hbar^2} \times \left[\frac{\sin(2k_F R) - 2k_F R\cos(2k_F R)}{(2k_F R)^4}\right], \tag{4}$$

where m^* is the effective mass of the carriers, J_{sd} is the Mn ion-free carrier exchange integral, a_0 is the lattice constant, N_Σ is the degeneracy of the Σ band, R is the distance between two Mn ions, and

$$k_F = \left(\frac{3\pi^2(p-p_c)}{N_\Sigma}\right)^{1/3} \tag{5}$$

is the Fermi wave number. This calculation of the Fermi wave number implies that any change of the carrier concentration in the L band is neglected for $p > p_c$. This assumption is well satisfied, due to the large difference in effective mass for both types of carriers.[25]

In this expression for the RKKY interaction, it is

assumed that the carriers in the material have an infinite mean free path. However, the carriers in $Pb_{0.28-x}Sn_{0.72}Mn_xTe$ and $Sn_{1-x}Mn_xTe$ are generated by vacancies in the lattice, which act as scattering centers for the carriers. This nonmagnetic disorder is therefore a source for dispersion of the RKKY interaction, which renders the exchange coupling between, e.g., nearest-neighbor pairs of spins into a statistical quantity. This results in a random phase of the oscillations of the RKKY function. For the calculations, we must average over this nonmagnetic disorder. It was already pointed out by de Gennes[31] that for large distances this averaging results in an exponential damping of the interaction, with a characteristic length scale λ. Usually, this exponential damping term is included in the interaction at all distances:

$$\overline{J}(R) = J_{\mathrm{RKKY}}(R)\exp\left(-\frac{R}{\lambda}\right) \qquad \text{for all } R. \tag{6}$$

For $R \lesssim \lambda$, however, it was shown theoretically that the nonmagnetic disorder does not significantly affect the RKKY interaction.[32–35] Therefore, we will approximate the real interaction, by an exponential damping of the RKKY interaction at distances $R > \lambda$, and the pure RKKY interaction at $R < \lambda$. The distance of $R = \lambda$, separating the two regimes, was chosen arbitrarily. Furthermore, we adjusted the exponential term to obtain a continuous function at $R = \lambda$. The interaction, averaged over the nonmagnetic disorder, is now

$$\overline{J}(R) = J_{\mathrm{RKKY}}(R), \quad R < \lambda, \tag{7a}$$

$$\overline{J}(R) = J_{\mathrm{RKKY}}(R)\exp\left(-\frac{R-\lambda}{\lambda}\right), \quad R > \lambda, \tag{7b}$$

where $J_{\mathrm{RKKY}}(R)$ is given by Eq. (4). To calculate ΔJ, the average over J^2 has to be known as well. This is given by

$$\overline{J^2}(R) = J^2_{\mathrm{RKKY}}(R), \quad R < \lambda, \tag{8a}$$

$$\overline{J^2}(R) = J^2_{\mathrm{RKKY}}(R)\exp\left(-2\frac{R-\lambda}{\lambda}\right) + \frac{1}{2}\left(\frac{m^* J_{sd}^2 a_0^6 k_F^4 N_\Sigma}{32\pi^3\hbar^2}\right)^2 \frac{1+4k_F^2R^2}{(2k_FR)^8} \times\left[1-\exp\left(-2\frac{R-\lambda}{\lambda}\right)\right], \quad R > \lambda. \tag{8b}$$

With this formulation, we will calculate the distributions of interactions in the material. The mean and width of these distributions will be used to calculate the transition temperatures and the phase boundary.

IV. DISTRIBUTION OF INTERACTIONS

To calculate the distribution of interactions, the total interaction an ion i experiences from its surrounding ions will be considered. In the spirit of SS, this is given by

$$J_i = \sum_{\text{all ions}} \overline{J}(R), \tag{9}$$

where $\overline{J}(R)$ is given by Eq. (7). For the distribution of interactions, all ions i must be taken. This is equivalent to taking one central ion, and considering all possible configurations of ions around this ion. These ions can be put into shells j, separated from the central ion by a distance $R_j = a_0\sqrt{j/2}$.[36] Each ion within such a shell interacts with the central ion with a strength $\overline{J}(R_j)$. Then

$$J_i = \sum_{j=1}^{N} n_{ij}\overline{J}(R_j). \tag{10}$$

Here n_{ij} is the number of ions present in shell j in the configuration corresponding to distribution i, N is the number of shells taken in the calculation ($N = 200$), and $\overline{J}(R_j)$ is taken from (7). The probability associated with this J_i equals the probability of the distribution:

$$P(J_i) = p_i = \prod_{j=1}^{N}\binom{z_j}{n_{ij}} x^{n_{ij}}(1-x)^{z_j-n_{ij}}, \tag{11}$$

where z_j is the number of lattice sites in shell j. By choosing $N = 200$, we have included all interactions within a sphere with a radius of $10a_0$. Because of the fast decrease of the RKKY interaction, a summation over larger distances contributes negligibly to the result. The effect of spin flips due to spin-orbit scattering or electron-phonon interactions is neglected as well, because they are expected to introduce still larger length scales at low temperatures.

Some of the calculated distributions, taking $\lambda = 1$ nm,[25] are shown in Fig. 3. The interaction strengths are scaled to the interaction strength at the nearest-neighbor position $[J(R_1)]$ to avoid uncertainties in the parameters determining the strength of the RKKY interaction. In Figs. 3(a)–3(c) the carrier concentration was kept constant at $p = 20 \times 10^{20}$ cm^{-3}, while the manganese concentration was changed ($x = 0.001$, 0.01, and 0.1). In Figs. 3(d)–3(f) the manganese concentration is kept constant at $x = 0.03$, while the carrier concentration was changed ($p = 5$, 20, and 50×10^{20} cm^{-3}). With a very low manganese concentration [Fig. 3(a)], the distribution is discrete, and the peaks correspond to the interaction strength at the lattice sites. The main peak of the distribution is situated at $J_i = 0$. If the manganese concentration is increased, the peaks first broaden and merge, because the lattice is filled more [Fig. 3(b)], and subsequently the distribution shifts to higher interaction strengths [Fig. 3(c)]. In this process, the main peak of the distribution first shifts to negative values of J_i, and subsequently to high positive values. At $x = 0.50$ the distribution is Gaussian, and above $x = 0.50$ the distribution gradually decomposes again into separate lines, ending in a discrete distribution near $x = 1.0$ (not shown). If the carrier concentration is increased [Figs. 3(d)–3(f)], the period of the RKKY interaction decreases, which re-

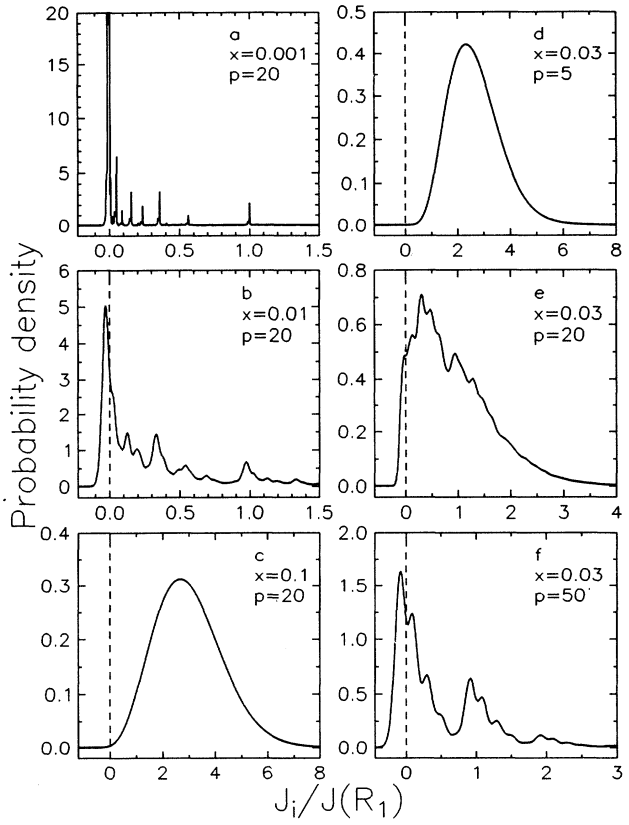

FIG. 3. Calculated distributions of interactions for various combinations of manganese and carrier concentrations. (a) $x = 0.001$, $p = 20 \times 10^{20}$ cm^{-3}; (b) $x = 0.01$, $p = 20 \times 10^{20}$ cm^{-3}; (c) $x = 0.1$, $p = 20 \times 10^{20}$ cm^{-3}; (d) $x = 0.03$, $p = 5 \times 10^{20}$ cm^{-3}; (e) $x = 0.03$, $p = 20 \times 10^{20}$ cm^{-3}; and (f) $x = 0.03$, $p = 50 \times 10^{20}$ cm^{-3}. The interaction strengths are scaled to the interaction strength at the nearest-neighbor position. The mean free path $\lambda = 1$ nm.

sults in a strong distance dependence of the interaction of the central ion with its first few neighbors. Therefore, if the manganese concentration is low, the distribution is dominated by these neighbors, resulting in a more structured distribution at high carrier concentrations.

Also in this case, the main peak of the distribution is found at $J_i < 0$. It thus turns out that the main peak of the distribution is situated at a negative total interaction if the manganese concentration is low and the carrier concentration is high. If the opposite is true, the main peak is situated at a positive total interaction. In the former case a spin-glass phase is expected, whereas in the latter case a ferromagnetic phase will occur. This is in good agreement with the experimental observations.

V. TRANSITION TEMPERATURES

We will now proceed with the results of the calculations of the transition temperatures, where we will consider the Curie temperature and spin-glass ordering temperature [Eq. (2)], as well as the Curie-Weiss temperature (Θ). For T_C and T_{SG} both J_0 and ΔJ must be known. These can be calculated from the distributions of interactions, but fortunately, it can also be done analytically, as

$$J_0 = \sum_i p_i J_i, \tag{12a}$$

$$(\Delta J)^2 = \sum_i p_i \overline{\left(\sum_{j=1}^{N} n_{ij} J(R_j) \right)^2} - \sum_i p_i J_i^2, \tag{12b}$$

with J_i taken from Eq. (10). This can be rewritten to

$$J_0 = x \sum_{j=1}^{N} z_j \overline{J}(R_j), \tag{13a}$$

$$\begin{aligned}(\Delta J)^2 = {} & (x - x^2) \sum_{j=1}^{N} z_j \overline{J^2}(R_j) \\ & + x^2 \sum_{j=1}^{N} z_j^2 \left[\overline{J^2}(R_j) - \overline{J}^2(R_j) \right] \\ & + x^2 \sum_{j=1}^{N} \sum_{\substack{k=1 \\ k \neq j}}^{N} z_j z_k \left[\overline{J(R_j) J(R_k)} - \overline{J}(R_j) \overline{J}(R_k) \right].\end{aligned} \tag{13b}$$

The first term in Eq. (13b) is due to the magnetic disorder, the second term appears only in the case of nonmagnetic disorder, and the third term stems from correlations between the magnetic and nonmagnetic disorder. These correlations are only present if the spatial distributions of vacancies and manganese ions are correlated. We will assume that these correlations are absent, by which the last term in Eq. (13b) vanishes.

The Curie-Weiss temperatures, which will also be considered, can be obtained from high-temperature series expansions as

$$\Theta = \frac{2S(S+1)x}{3k_B} \sum_{j=1}^{\infty} z_j \overline{J}(R_j) = \frac{2S(S+1)}{3k_B} J_0. \tag{14}$$

Since the sums in Eq. (13b) only depend on the carrier concentration, the contributions from the carrier and manganese concentration to the transition temperatures can be investigated separately. It is now clear that the model predicts that Θ is proportional to x, T_C is proportional to x only if $\eta^2 \gg 12/35$, which is already reasonably well established when the ferromagnetic phase occurs ($\eta > 40/\sqrt{1295}$), and that T_{SG} is proportional to $\sqrt{x}$ for low values of $x (\ll 1)$.

In Fig. 4 the calculations of Θ/x are compared to the experimental data. To investigate the influence of the mean free path of the carriers, two values for λ are taken: $\lambda = 1$ nm and $\lambda = \infty$. The magnitude of the Curie-Weiss temperature was fitted to the data, taking $m^* = 1.7 m_e$,[25] and using J_{sd} as a fitting parameter. This yielded $J_{sd} = 65$ meV for both values of λ. Both curves describe the experimental data reasonably well, although

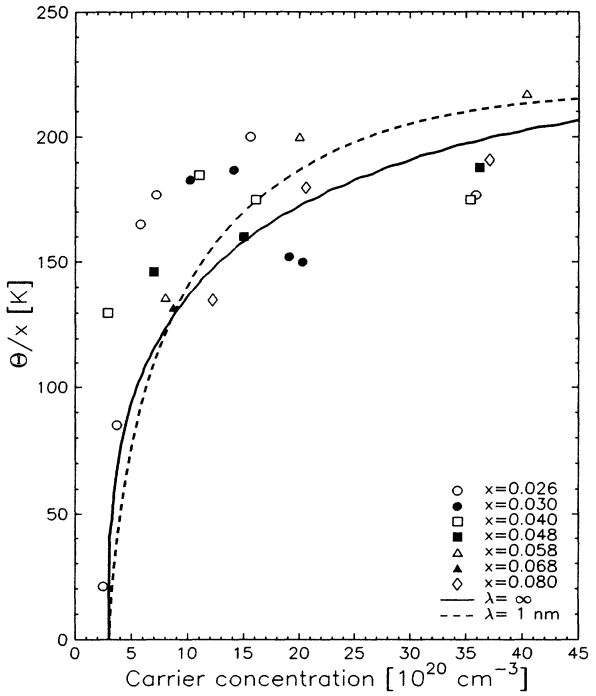

FIG. 4. Curie-Weiss temperature scaled to the manganese concentration versus the carrier concentration for samples of $Sn_{1-x}Mn_xTe$ with x ranging from 0.026 to 0.080. The curves are calculations based on the SS model. Solid curve, $\lambda = \infty$; dashed curve, $\lambda = 1$ nm.

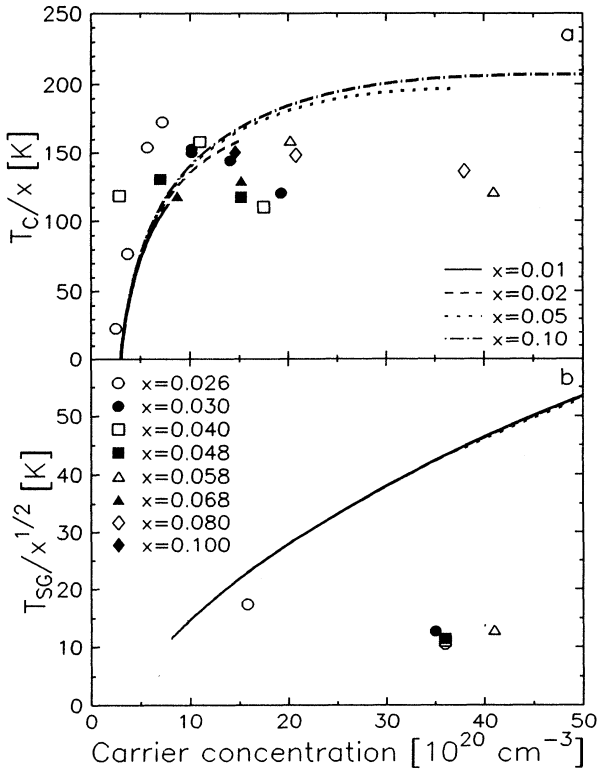

FIG. 5. T_C/x (a) and $T_{SG}/\sqrt{x}$ (b) as a function of the carrier concentration. Lines represent the calculations for $\lambda = 1$ nm; markers represent the experimental data.

the calculated transition to the paramagnetic state is not as sharp as observed experimentally. The value of J_{sd} compares well with reported values, which range from 33 meV, obtained from electron paramagnetic resonance experiments,[37] to 100 meV, also obtained from Curie-Weiss temperatures, but using a different model.[38] We will use the value of J_{sd} obtained in this description for the calculations in the rest of this paper.

T_C/x and $T_{SG}/\sqrt{x}$, calculated for $x = 0.02$, 0.05, and 0.10 with $\lambda = 1$ nm, are shown together with our experimental data in Fig. 5. The calculated lines are only shown in the regime where they are valid, according to the SS phase diagram (Fig. 2). As predicted, the calculations of T_C [Fig. 5(a)] approximately scale with x in the regime where the ferromagnetic phase occurs. Compared to the experimental results, the magnitude of T_C is somewhat too high, especially at high carrier concentrations. It must be noted, however, that the relative uncertainty in the experimental data is roughly 10%, due to the inaccuracy of the determination of the manganese concentration. The difference between the calculations and the experiments at high carrier concentrations is not unexpected, because the calculated Curie-Weiss temperature is also too large at these carrier concentrations, and the difference between the Curie-Weiss temperature and the Curie temperature in the calculations is only small.

The calculated spin-glass temperatures [Fig. 5(b)] indeed scale with $\sqrt{x}$, as expected. However, the curves fail to describe the experimental data. This can be attributed to the fact that the SS model predicts a spin-glass phase if $T_{SG} > T_C$, whereas the experimental freezing temperatures are much lower than the Curie or Curie-Weiss temperatures. Moreover, the experimental freezing temperatures appear to scale roughly with x instead of $\sqrt{x}$.[14]

Nevertheless, the model does describe other experimental features. This can be seen in Fig. 6, where the calculated transition temperatures are plotted versus the manganese concentration for three different carrier concentrations, together with experimental data on samples with approximately the same carrier concentrations. To describe the experimental data we discern different temperatures: the Curie temperature (T_C) for ferromagnetic and reentrant-spin-glass samples, the freezing temperature (T_{SG}) for spin glasses, and the temperature of the ferromagnetic-to-spin-glass transition ($T_{FM\text{-}SG}$) for reentrant spin glasses. $T_{FM\text{-}SG}$ cannot be described with the SS model, but is included in the diagrams to facilitate the comparison with results on other reentrant-spin-glass systems, like *Au*Fe and *Pd*Mn (Refs. 11, 8, 22), and earlier results in this system.[28,39] For the calculated curves we have only shown the higher of the Curie and spin-glass temperatures. The crossover from T_{SG} at low manganese concentrations to T_C at high manganese concentrations is indicated by the arrows.

For $p \approx 7 \times 10^{20}$ cm^{-3} [Fig. 6(a)] the model predicts a

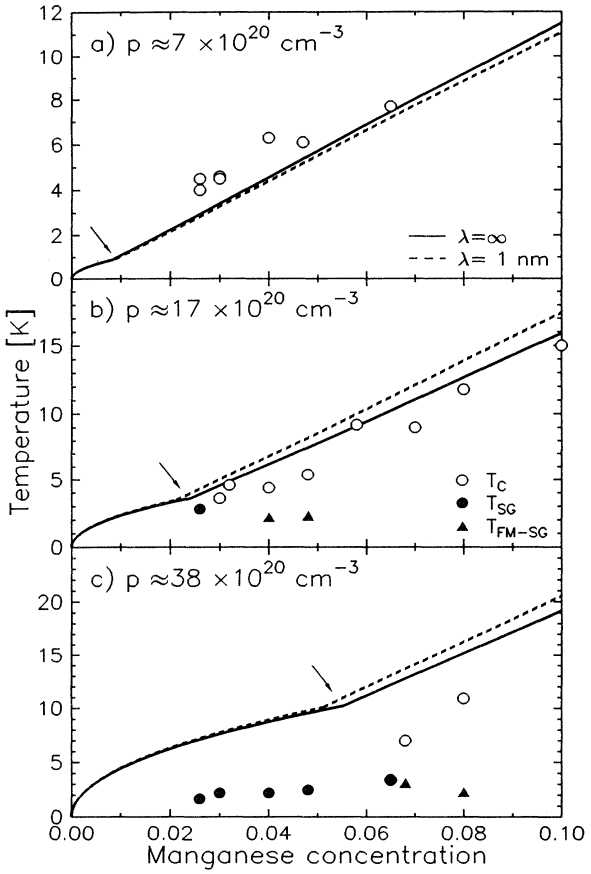

FIG. 6. Transition temperatures as a function of the manganese concentration for $p \approx 7 \times 10^{20}$ cm^{-3} (a), $p \approx 17 \times 10^{20}$ cm^{-3} (b), and $p \approx 38 \times 10^{20}$ cm^{-3} (c). The curves represent the calculations with the SS model; markers represent the experimental results. Solid curve, $\lambda = \infty$; dashed curve, $\lambda = 1$ nm. Open circles, Curie temperature; solid circles, spin-glass temperature; solid triangles, ferromagnetic-to-spin-glass transition temperature.

phase transition at approximately $x = 0.01$. All our data are for $x \geq 0.026$ and show a ferromagnetic transition. This is in accordance with the model, but as there are no data available around the transition point, we cannot test its location. For $p \approx 17 \times 10^{20}$ cm^{-3} [Fig. 6(b)] the calculated point for the phase transition coincides with the experimental point. It must be noted that the experiments on the sample with $x = 0.026$, pictured as a spin glass, indicate that it may also be interpreted as a reentrant spin glass, in which the temperatures T_C and $T_{\text{FM-SG}}$ are so close that the two transitions merge into a single transition. The magnetic phase of this sample can therefore not be determined unambiguously. For high carrier concentrations [$p \approx 38 \times 10^{20}$ cm^{-3}, Fig. 6(c)] the magnitude of the calculated temperatures is too high, but the transition point is predicted at approximately the correct manganese concentration. At this carrier concentration, the magnetic phase of the sample with $x = 0.065$ cannot be determined unambiguously, just like the sample with $x = 0.026, p \approx 17 \times 10^{20}$ cm^{-3} described above. The experimental phase diagrams presented in Fig. 6(b) and Fig. 6(c) are in quantitative agreement with those reported by Mauger and co-workers,[28,39] and qualitatively resemble those in *Au*Fe and *Pd*Mn.[11,8,22] The shape of the calculated curve resembles that of the measurements. The differences between the curves with different λ's are again not so large.

Now that we have seen that the transition from spin glass to ferromagnet can be described reasonably well at these carrier concentrations, we will proceed to calculate the phase transition in the x-p phase diagram, and compare it to the experimental data.

VI. BOUNDARIES IN THE x-p PHASE DIAGRAM

In this section we will describe the phase boundary in the x-p phase diagram using two different approaches. First, a previously reported geometrical argument will be refined, and subsequently the SS model will be used.

As argued before (Sec. IV and Ref. 13) a ferromagnetic phase may be expected if the ferromagnetic onset of the RKKY interaction is most important. Therefore, a phase transition is expected when the distance at which the RKKY interaction changes sign (R_{RKKY}) equals the average distance at which a Mn ion has its nearest magnetic neighbor ($\overline{R_{\text{Mn}}}$).[13] This conclusion was also reached by Mauger and Escorne[39] based on a percolation argument.

R_{RKKY} is determined from Eq. (4):

$$R_{\text{RKKY}} = \frac{4.49}{2k_F}, \tag{15}$$

where k_F is given by Eq. (5).

The average Mn distance is obviously determined by the concentration of magnetic ions. However, to calculate $\overline{R_{\text{Mn}}}$ is not straightforward. Previously, this was determined by calculating the cubic root of the mean volume (volume model), yielding[13,39]

$$\overline{R_{\text{Mn}}} = R_1 x^{-1/3}. \tag{16}$$

This is equivalent to placing all ions on a virtual fcc lattice, with a nearest-neighbor distance $\overline{R_{\text{Mn}}}$. The distribution of ions over the real lattice is, however, not regular. This will affect the average distance at which a magnetic neighbor is found. Therefore, we adopted a more realistic way to calculate $\overline{R_{\text{Mn}}}$ by performing a sum over shells surrounding a central ion (shell model). As we are only interested in the nearest magnetic neighbor, a shell is taken into account only if it contains ions, and all inner shells are empty:

$$\overline{R_{\text{Mn}}} = R_1[1-(1-x)^{z_1}] + R_2(1-x)^{z_1}[1-(1-x)^{z_2}] + \cdots + R_N(1-x)^{z_1+\cdots+z_{N-1}}[1-(1-x)^{z_N}], \tag{17}$$

where $(1-x)^{z_j}$ is the probability that shell j is empty.

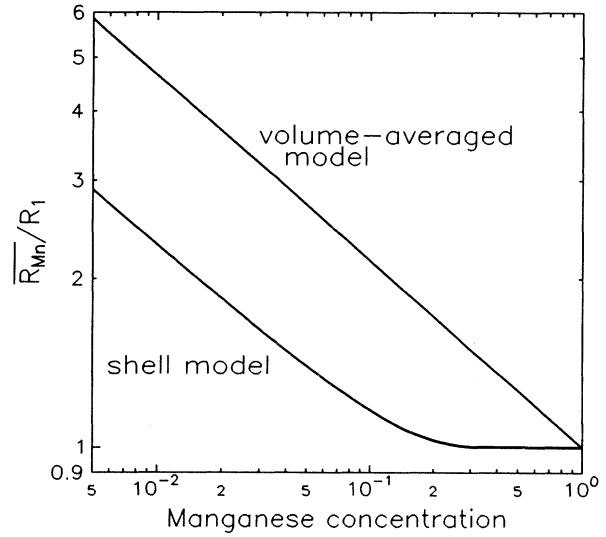

FIG. 7. Average nearest-magnetic-neighbor distance, scaled to the nearest-neighbor distance, versus the manganese concentration calculated for both our models (see text).

In Fig. 7 this average distance is shown in a log-log plot together with the distance calculated from the average volume [Eq. (16)]. The difference between the two curves is striking. At low manganese concentrations, both approaches yield an average distance approximately proportional to $x^{-1/3}$, but in the shell model it is already close to the nearest-neighbor distance at $x \approx 0.20$, the percolation limit for the fcc lattice. This is consistent with the intuitive picture that a ferromagnetic phase should occur above the percolation limit if a strong ferromagnetic nearest-neighbor interaction is present. The difference between the two approaches is due to the difference between $\overline{R^3}$ (volume model) and $\overline{R}^3$ (shell model). This difference arises from the random distribution of the Mn ions over the cation sublattice. Since we consider only the nearest neighbor of each ion, short distances are favored over long distances, thereby reducing the average distance with respect to the virtual lattice used for the volume model.

The phase boundary in the x-p phase diagram was calculated by equating $\overline{R_{\mathrm{Mn}}}$ [Eq. (17)] and R_{RKKY} [Eq. (15)] This boundary is shown in Fig. 1 as the dotted curve. If this curve is compared to the curve calculated with Eq. (16) (see Ref. 13), it has shifted towards lower manganese concentrations, thereby missing the data by an order of magnitude. This intuitive model does therefore not describe the data accurately, in spite of earlier claims.[13]

In the SS model, the phase boundary is determined by the relation $T_{\mathrm{SG}} = T_C$, yielding $\eta = J_0/\Delta J = 40/\sqrt{1295}$, where J_0 and ΔJ are calculated with Eq. (13). As η is given by the ratio of J_0 and ΔJ the phase boundary does not depend on the magnitude of the RKKY interaction or, more specifically, on the value of J_{sd}. The lines thus obtained are also shown in Fig. 1. The model describes the experimental data well. The effect of the finite value of λ on the phase boundary is not so large. This is caused by two opposing effects of the mean free path. A short mean free path reduces the influence of the outer shells with respect to the inner shells. This will reduce both the mean and the width of the distribution of interactions. Their ratio does not change too much, and therefore the net effect on the phase boundary is not so large. Furthermore, the mean free path reduces the interaction strength only at distances beyond $R = \lambda$, which is beyond the fifth neighbor. An important part of the total interaction strength is then already built up.

VII. DISCUSSION AND CONCLUSIONS

In this paper, we presented a model description of the ferromagnet-to-spin-glass transition in a diluted magnetic system with an RKKY interaction, based on the model by Sherrington and Southern. Due to the dominance of the RKKY interaction, the free carrier density is an important parameter in the system. The model was applied to $Sn_{1-x}Mn_xTe$ and $Pb_{0.28-x}Sn_{0.72}Mn_xTe$, a system that is very suitable to study the RKKY interaction because of the importance of both the free carrier density and the manganese concentration. Nevertheless, it can in principle be applied to any system in which the magnetic behavior is dominated by the RKKY interaction.

The SS model was chosen for the description, because it was developed for a system with a short-ranged interaction. Although the RKKY interaction is long ranged, its range is greatly reduced by the short mean free path of the carriers in our system. If the mean free path is longer, the SK model may be preferred above the SS model. However, the formulations are different and in the SK model only $S = 1/2$ magnetic moments are considered. The SK formulation is not easily transformed to include a general spin of the magnetic moments. An advantage of the SK model is the possibility to describe the transition from the ferromagnetic to the spin-glass state by means of the de Almeida–Thouless formalism.[40] This transition is attributed to the instability of the ferromagnetic phase at low temperatures. The stability of the SS model is not investigated up to now, which hampers the description of the ferromagnetic-to-spin-glass transition temperature. It is, however, conceivable that an instability will occur in the SS model as well. This means that the phase boundary we have calculated is in fact the boundary separating the spin-glass and reentrant-spin-glass regimes. The transition to the ferromagnetic state should occur at a higher value of η, which results in a phase boundary positioned at lower carrier concentrations with respect to the boundaries plotted in Fig. 1.

In the model the valence band is assumed to be isotropic, and interactions between the various valence band maxima are neglected. These effects were shown to render an anisotropic RKKY interaction.[41] In that case the first switch from a ferromagnetic to an antiferromagnetic interaction is expected to occur at a shorter distance, which favors the formation of a spin-glass phase.

These effects were not included, because of an increase of the number of unknown interaction parameters, and a large numerical complication of the model. The influence of the antiferromagnetic superexchange mechanism was also not considered. The superexchange mechanism will reduce the interaction at the nearest-neighbor position,[24] again favoring the formation of a spin-glass phase. It is further possible that the mean free path of the carriers also depends on the concentration of those carriers, because the carriers are generated by vacancies in the host lattice. A high carrier concentration therefore implies a high vacancy concentration, which reduces the mean free path of the carriers. This favors the ferromagnetic phase at high carrier concentrations, because the interaction will be limited to the first few, ferromagnetically coupled neighbors. The combined effect of these effects still demands further theoretical study.

To conclude this paper, we will summarize our main results. Using our model, we calculated the distributions of interactions in the material. The magnetic phase predicted by these distributions is in good agreement with the experimental observations. Using the mean and width of these distributions, the Curie-Weiss constant, as well as the Curie temperature and the spin-glass ordering temperature, can be calculated. The calculated Curie-Weiss constant could be fitted to the measured temperatures reasonably well. Using the results from these fits, the calculated Curie temperatures were also in reasonable accordance with the experiments. The calculated spin-glass temperatures were, however, much higher than the experimental temperatures. This is attributed to an inconsistency in the SS model. Subsequently, the transition points from spin-glass behavior to ferromagnetism can be used to compile a phase boundary in the x-p phase diagram. This boundary describes the experimental results quite well. The length of the mean free path of the carriers did not significantly affect the results.

ACKNOWLEDGMENTS

The authors thank Dr. C.W.H.M. Vennix for stimulating discussions. The research of H.J.M.S. was supported by the Royal Netherlands Academy of Arts and Sciences; the research of T.S. was supported by KBN (Grant No. 2 0482 91 01) and NSF/PAN (Grant No. 92-113).

[1] H. Maletta, G. Aeppli, and S.M. Shapiro, Phys. Rev. Lett. **48**, 1490 (1982).
[2] J.K. Furdyna, J. Appl. Phys. **64**, R29 (1988).
[3] W.J.M. de Jonge and H.J.M. Swagten, J. Magn. Magn. Mater. **100**, 322 (1991).
[4] *Diluted Magnetic Semiconductors*, edited by J.K. Furdyna and J. Kossut, Vol. 25 of *Semiconductors and Semimetals* (Academic Press, Boston, 1988).
[5] J. Kossut and W. Dobrowolski, in *Handbook of Magnetic Materials*, edited by K.H.J. Buschow (North-Holland, Amsterdam, 1993), Vol. 7, p. 231.
[6] B.E. Larson, K.C. Hass, H. Ehrenreich, and A.E. Carlsson, Phys. Rev. B **37**, 4137 (1988).
[7] P.W. Anderson, Phys. Rev. **155**, 1 (1959).
[8] J.A. Mydosh and G.J. Nieuwenhuys, in *Ferromagnetic Materials*, edited by E.P. Wohlfarth (North-Holland, Amsterdam, 1980), Vol. 1, p. 71.
[9] J.A. Mydosh, *Spin Glasses* (Taylor & Francis, London, 1993).
[10] M.A. Ruderman and C. Kittel, Phys. Rev. **96**, 99 (1954); T. Kasuya, Prog. Theor. Phys. **16**, 45 (1956); K. Yosida, Phys. Rev. **106**, 893 (1957).
[11] G.J. Nieuwenhuys, B.H. Verbeek, and J.A. Mydosh, J. Appl. Phys. **50**, 1685 (1979).
[12] B.H. Verbeek, G.J. Nieuwenhuys, H. Stocker, and J.A. Mydosh, Phys. Rev. Lett. **40**, 586 (1978).
[13] W.J.M. de Jonge, T. Story, H.J.M. Swagten, and P.J.T. Eggenkamp, Europhys. Lett. **17**, 631 (1992).
[14] C.W.H.M. Vennix, E. Frikkee, P.J.T. Eggenkamp, H.J.M. Swagten, K. Kopinga, and W.J.M. de Jonge, Phys. Rev. B **48**, 3770 (1993).
[15] D. Sherrington and S. Kirkpatrick, Phys. Rev. Lett. **35**, 1792 (1975); S. Kirkpatrick and D. Sherrington, Phys. Rev. B **17**, 4384 (1978).
[16] M.W. Klein, Phys. Rev. **173**, 552 (1968); Phys. Rev. B **14**, 5008 (1976).
[17] P.J.T. Eggenkamp, T. Story, H.J.M. Swagten, C.W.H.M. Vennix, C.H.W. Swüste, and W.J.M. de Jonge, Semicond. Sci. Technol. **8**, S152 (1993).
[18] P.J.T. Eggenkamp, C.W.H.M. Vennix, T. Story, H.J.M. Swagten, C.H.W. Swüste, and W.J.M. de Jonge, J. Appl. Phys. **75**, 5728 (1994).
[19] D. Sherrington and B.W. Southern, J. Phys. F **5**, L49 (1975).
[20] S.F. Edwards and P.W. Anderson, J. Phys. F **5**, 965 (1975).
[21] I.A. Campbell, Phys. Rev. Lett. **68**, 3351 (1992).
[22] G.J. Nieuwenhuys, Phys. Lett. **67A**, 237 (1978).
[23] U. Larsen, Solid State Commun. **22**, 311 (1977); Phys. Rev. B **18**, 5014 (1978).
[24] T. Story, G. Karczewski, L. Świerkowski, and R.R. Gałązka, Phys. Rev. B **42**, 10477 (1990).
[25] G. Karczewski, L. Świerkowski, T. Story, A. Szczerbakow, J. Niewodniczańska-Blinowska, and G. Bauer, Semicond. Sci. Technol. **5**, 1115 (1990).
[26] R.R. Gałązka, J. Spałek, A. Lewicki, B.C. Crooker, G. Karczewski, and T. Story, Phys. Rev. B **43**, 11093 (1991).
[27] M. Godinho, J-L. Tholence, A. Mauger, M. Escorne, and A. Katty, in *Proceedings of the 17th International Conference on Low Temperature Physics*, edited by H. Eckern, A. Schmid, W. Weber, and H. Wühl (Elsevier, Amsterdam, 1984), p. 647.
[28] M. Escorne, M. Godinho, J-L. Tholence, and A. Mauger, J. Appl. Phys. **57**, 3424 (1985).
[29] T. Story, R.R. Gałązka, R.B. Frankel, and P.A. Wolff, Phys. Rev. Lett. **56**, 777 (1986).
[30] H.J.M. Swagten, W.J.M. de Jonge, R.R. Gałązka, P. Warmenbol, and J.T. Devreese, Phys. Rev. B **37**, 9907 (1988).
[31] P.G. de Gennes, J. Phys. Radium **23**, 630 (1962).

[32] A. Yu. Zyuzin and B.Z. Spivak, JETP Lett. **43**, 234 (1986).
[33] L.N. Bulaevskiĭ and S.V. Panyukov, JETP Lett. **43**, 240 (1986).
[34] A. Jagannathan, E. Abrahams, and M.J. Stephen, Phys. Rev. B **37**, 436 (1988).
[35] I.V. Lerner, Phys. Rev. B **48**, 9462 (1993).
[36] In these systems $a_0 = 0.63$ nm (Ref. 24).
[37] T. Story, P.J.T. Eggenkamp, C.H.W. Swüste, H.J.M. Swagten, W.J.M. de Jonge, and A. Szczerbakow, Phys. Rev. B **47**, 227 (1993).
[38] T. Story, G. Karczewski, L. Świerkowski, M. Górska, and R.R. Gałązka, in Proceedings of the International Conference on the Narrow Gap Semiconductors and Related Materials, Gaithersburg, 1989 [Semicond. Sci. Technol. **5**, S138 (1990)].
[39] A. Mauger and M. Escorne, Phys. Rev. B **35**, 1902 (1987).
[40] J.R.L. de Almeida and D.J. Thouless, J. Phys. A **11**, 983 (1978).
[41] T. Story, P.J.T. Eggenkamp, C.H.W. Swüste, H.J.M. Swagten, W.J.M. de Jonge, and L.F. Lemmens, Phys. Rev. B **45**, 1660 (1992), and references therein.